https://erjm.journals.ekb.eg
ISSN: 1110-1180

DOI: ---------

ERJ
Engineering Research Journal
Faculty of Engineering
Menoufia University

Numerical Study for The Behavior of Novel Concrete Filled Built-Up Cold Formed Steel Columns Under Compression Load

Magdy I. Salama [1], Galal A. Elsamak [1,2], Mohammed A. Shousha [1,*], Boshra A. Eltaly [3]

[1] Civil Engineering Department, Faculty of Engineering, Kafrelsheikh University, Kafrelsheikh, Egypt
[2] Department of Civil Eng., Delta Higher Institute for Engineering & Technology, Talkha, Egypt
[3] Civil Engineering Department, Faculty of Engineering, Menoufia University, Shebin El-kom, Egypt.
**(Corresponding author: mohamed_shosha2015@eng.kfs.edu.eg).*

ABSTRACT
Concrete filled built-up cold-formed steel columns (CF-BCFSCs) have a widespread in the applications of high-rise constructions and heavy bearing structures. This paper presents a numerical study depending on finite element (FE) method using Abaqus software to study the behavior of CF-BCFSCs under axial compression load. The current study presents the numerical model taking into consideration the interaction between the steel skin and the infill concrete core, material nonlinearity, modeling of confined concrete, and geometric nonlinearity. The proposed FE model is validated by aligning its results with those obtained from a previous experimental study documented in the literature, demonstrating good agreement. A parametric numerical investigation of four innovative CF-BCFSCs was conducted to explore the impact of a wider array of variables, including cross-sectional configurations, ultimate-load capacity, cost-effectiveness, buckling patterns, the ultimate load contribution of the steel skin and the in-filled concrete core. Local and distortional buckling are the major mode of failures for most columns, while the overall buckling does not occur. Based on finite element results, the square column from U and C channels (S-U+C) produce the maximum ultimate load, and the most cost-effectiveness column, and the rectangular column from U and Σ channels RU+ Σ shows the highest ductility, and finally the square column from U and Σ channels (S-U+Σ) has the highest elastic stiffness.
Keywords*: Concrete filled column, Concentric compression, Cold formed steel, Confined concrete, Numerical model.*

1. Introduction

Concrete-filled steel tube (CFST) columns combine the best of steel and concrete: the steel's confinement boosts the concrete's strength and flexibility, while the concrete core prevents the steel tube from buckling early [1]. This powerful combo offers several advantages over traditional steel and concrete columns including higher load-bearing capacity and stiffness, greater ductility, higher slenderness ratio, enhanced durability, and reduced construction time and cost [2]. This makes CFST columns ideal for demanding structural applications including high-rise buildings, bridges, offshore platforms, industrial facilities, sports stadiums, airports, and railway stations and power plants [3], Figure (1). Iconic structures like Burj Khalifa and Millau Viaduct stand as testaments to the power of CFST technology.

Various design standard Codes, such as EN 1994-1-1 [4], the Australian Standards AS 5100 [5], JGJ 138 [6], the American ANSI/AISC [7], and the Chinese regulations DBJ/T 13-5 [8] specifically tackle the topic of CFST. Many previous researchers have conducted intensive studies on the impact of the shape of the outer steel skin utilizing common simple geometric patterns rectangular, and circular shapes. For example, Kazemzadeh et al. [9–١1] examined slenderness limits under axial load along with local and post-local buckling of composite columns filled with concrete. Their study encompassed various designs for different cross section shapes including box, circular, and partially encased I-sections. The study concluded that local buckling is the primary mode of failure for short CFST columns.

Regarding enhancement of CFST behavior using high strength material, Xiong et al. [12] explored the axial behaviors of CFST made of ultra-high-strength concrete and steel. This study found that the EN 1994-1-1 [4] yields conservative outcomes when the confinement effect is ignored.

In recent times, researchers have increasingly focused on sustainable corrosion-resistant materials, such as stainless steel. Hassanein et al. [13,14] studied the behaviors of circular CFST stainless columns under axial load employing lean duplex stainless steel for the outer skin tube. Their findings, when compared to data from EN 1994-1-1 [4], suggested that EN 1994-1-1 [4] predictions were somewhat non-conservative for columns of intermediate length. Separately, Dabon et al. [15,16] explored the confinement influence on CFST short stainless columns, noting that the predictions according to ANSI/AISC [7] are extremely conservative. Through experiments and numerical modeling, Han et al. [17–21] incorporated carbon steel and stainless steel in short and long CFST. Their study proved that columns with stainless steel exhibited greater ductility and improved post-buckling.

Figure 1- Uses of CFST columns

In recent decades, there has been a significant rise in the utilization of composite built-up steel cross-sections in construction to overcome limitations associated with simple hot-rolled sections. Cold-formed steel (CFS) sections, undergoing plastic deformations that result in improved strain hardening and higher strength-to-weight ratios, make them suitable for light steel framing with increased load capacity [22]. Advances in novel cross-section configurations built-up from CFS are anticipated to enhance overall structure performance. Scholars highlight the distinct structural characteristics of various tubular cross-sectional shapes related to strength, ductility, failure mode, and providing different degrees of confinement to the concrete core [23–27]. Ellobody [28–30] conducted experiments on high-strength CFS tubed columns in-filled with concrete, comparing outcomes to those from EN 1994-1-1 [4] and AS5100 [5]. The study proved that AS5100 [5] offered more conservative estimates, while the European standard was typically less conservative.

Rahnavard et al. [31–32] undertook a study on the compressive behavior of innovative CF-BCFSCs. The research, incorporating experimental tests, aimed to evaluate the applicability of EN 1994-1-1 [4] in predicting buckling resistance, particularly for thin-walled steel. Through testing twelve columns, the study reported comprehensive findings that exposed inaccuracies in the EN 1994-1-1 [4] formulation in estimating steel contributions. Subsequently, the researchers proposed a modification in calculating the effective cross-sectional areas.

The literature reveals limited studies on the behavior of CF-BCFSCs under axial compression load. Current guidelines do not adequately address built-up thin-walled CFS designs in creating CF-BCFSCs. Additionally, obtaining a trusted and simple FEM model representing the interaction between CFS and infill concrete core, along with accurately modeling confined concrete, poses challenges. This research aims to investigate the behavior of four novel CF-BCFSCs under compressive loads, using a numerical approach extended from a previous experimental investigation by Rahnavard et al. [31]. The numerical model, created with Abaqus software

[33], considers the interaction between external steel skin elements and filling concrete, material nonlinearity, confined concrete modeling, and geometric nonlinearity. The proposed model's validity is confirmed by comparing numerical outputs with experimental results from the prior study [31]. The study aims to elucidate compressive dynamics, including load-bearing capacity, cross-sectional configurations, cost-effectiveness, buckling patterns, ductility, and the percentage contribution of the steel and the filled concrete components to the overall maximum resistance of the column.

2. **Finite element modeling**

The FE method has become increasingly popular for modeling CFST columns, thanks to advances in commercial software like Abaqus. This allows for accurate simulation of the steel-concrete interaction, considering imperfections, boundary conditions, and residual stresses. However, the accuracy of the FE model heavily relies on choosing the right concrete model, which is crucial for reliable predictions. This study employed Abaqus 2017 [33] to create a FE model of CF-BCFSCs stub columns. Here are the descriptions of two experimental previous studies that will be used to verify the numerical model proposed by the authors.

2.1 Description of the considered experimental studies

2.1.1 Experimental study by Rahnavard et al. [31]

A numerical model was created in Abaqus software extended from the experimental work by Rahnavard et al. [31] on the influence of axial compressive load on four new CF-BCFSCs sections. These sections were built using three profiles (C, U, and Σ) from CFS S280GD, and filled with lightweight concrete, 1850 kg/m3 density. Four built-up configurations were tested: 1-square with U and C profiles (S-U+C), 2-square with U and Σ profiles (S-U+ Σ), 3-rectangular with U and Σ profiles (R-U+ Σ), and 4-rectangular with U and C profiles (R-U+C). All specimens were 1050 mm long with fastener spacing 237.5 mm and end distance 50 mm. The geometry of CFS profiles and the column sections configurations are shown in Figure (2) and the test matrix is obvious in Table 1.

The properties of the materials composing the columns (steel and filled concrete) were taken from Rahnavard et al. [31] in the form of stress-strain curves, as shown in Figure (3). The elastic modulus and Poisson's ratio of steel and concrete are equal to Es=204.18 GPa and Ec=31.476 GPa and νs= 0.3 and νc=0.18, respectively. The yielding and ultimate stress of the steel equal 306.81 and 424.04 MPa, while the ultimate strength of the concrete in tension and compression equal 2.56 and 33 MPa.

As explained from the test set up in Figure (2), the specimens were positioned with vertical alignment in the hydraulic testing machine and loaded by a displacement control until failure. To prevent premature local buckling failure at the column ends, a clamping device was fabricated and assembled to both ends of the columns. Six LVDTs and strain gauges were used to measure the deformations and strains along the length of the column. Considering the frictional resistance applied by the testing apparatus, the column ends are restricted excluding vertical displacement at the top loaded end.

Table1: Test matrix

Column	Cold Formed profiles			Corner distance of Fasteners (mm)			*A*s (mm2)	A_c (mm^2)
	Σ	U	C	h_1	h_2	h_3		
S-U+C	-	2	2	-	21.5	-	1485	21 720
S-U+Σ	2	2	-	-	21.5	11.5	1540	18 307
R-U+Σ	2	2	-	-	21.5	11.5	1540	8912
R-U+C	-	2	2	39	23	-	1485	12 121

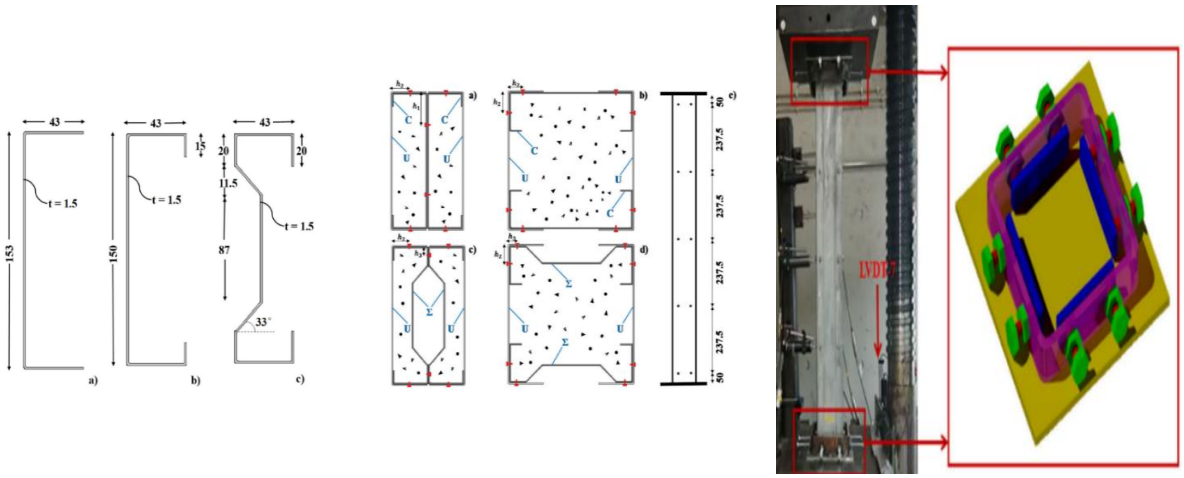

I II III

Figure 2- I. Geometry of CFS profiles (unit in mm); (a) U-shaped, (b) C-shaped, and (c) Σ-shaped, II. Built-up cross-sections configurations (unit in mm); (a) R-U+C, (b) S-U+C, (c) R-U+Σ, (d) S- U+Σ, (e) fastener spacing along the length,III. The Test set-up by Rahnavard etal [31]

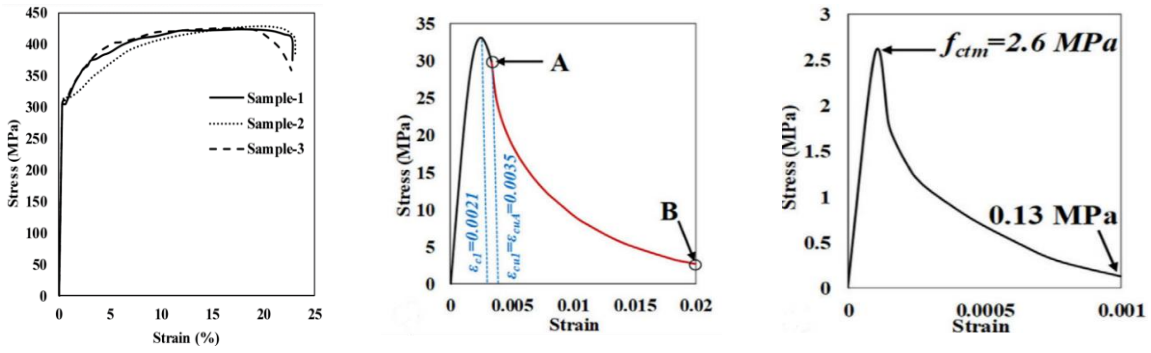

(a) (b) (c)

Figure 3- Material properties by Rahnavard etal [31]; a- Tensile coupon test results, b- compression behavior of concrete, c- Tension behavior of concrete

2.1.2. Experimental study by Teoh et al. [34]

Teoh et al. [34] presented an experimental investigation on 32 CF-BCFSCs stub columns composed of two front-to-front asymmetric lipped channels with stiffened web sections connected by rivets under concentric loading as shown in Figure (4). These specimens exhibited two distinct cross-sectional profiles determined by web depth (75 and 100 mm) encompassing different thicknesses. The outer steel skin is lipped channel sections made from steel grade G550 from CFS with nominal yield stress of 550 MPa, elastic modules 200.1Gpa, and poison ratio 0.24. The infilled core is from lightweight expanded concrete using clay aggregate with different compressive strength 22.7 Mpa and 40.3 Mpa. The mechanical properties of the steel skin and the concrete core in elastic and plastic zones are taken from Teoh et al. [34] research.

The experimental test set-up was done using 1000 kN testing machine that employed axial compression to the columns at a constant rate of 0.5 mm/min. Two linear variable differential transducers (LVDTs) and four pairs of strain gauges were used to observe post-buckling behavior. 10 mm thick steel plates were attached to both ends of the specimens to prevent local or 'elephant foot' failure at the column ends. The current study chooses two samples from Teoh et al. [34] research to be simulated numerically to verify numerical model these two samples are 102×51×1-LC20 and 75×40×0.75-LC40, where the first three letters represent the web length, flange width, and sheet thickness, respectively.

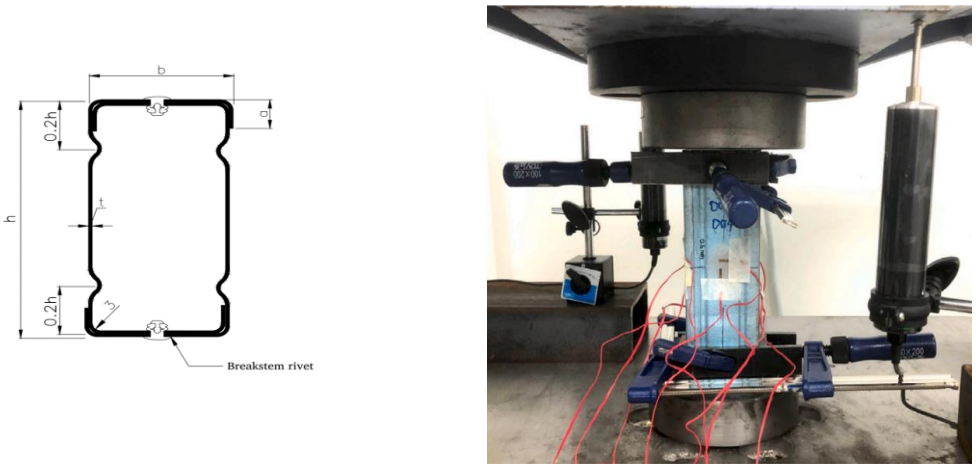

(a) (b)

Figure 4- a. Built-up cross-sections configurations, b. The Test set-up by Teoh et al [34]

2.2 Modeling by Abaqus

2.2.1. Modeling of steel material

This study used elastic-plastic with hardening model to characterize steel behavior. To enhance precision, the engineering stress-strain curves from the tensile steel coupon test by Rahnavard et al. [31] and Teoh et al [34] are transformed into true stress-strain curves using equations by Chen et al [35].

2.2.2. Modeling of concrete material.

The concrete damaged plasticity model in Abaqus was used to model the concrete core which model concrete nonlinearity as plasticity for compression and tensile behaviors. The key material parameters that determined for concrete model are presented by Tao et al. [35] included, the flow potential eccentricity (e) = 0.1 and the viscosity parameter = 1e-5.

The ratio of the compressive strength under biaxial loading to uniaxial compressive strength (f_{b0}/f_c') was determined from the equation proposed by Papanikolaou and Kappos [37] and found to be 1.163. While the ratio of the second stress invariant on the tensile meridian to that on the compressive meridian (Kc) can be determined according to Yu et al. [38] and found to be 0.703.

The dilation angle (ψ) is a parameter used in Abaqus controls how much concrete expands laterally when it is compressed. A sensitivity analysis was carried out to enhance the precision of the dilation angle. Various angles: 10, 20, 30, 40, and 50 degrees were systematically chosen for assessment. The parametric study indicated that increasing the dilation angle can result in a more ductile behavior; while decreasing it can lead to a more brittle behavior. In CFST columns, where the concrete is confined due to encasing by steel skin, it was found that larger values of the angle are more logical and accurate. A value of 40° is recommended to gives the best prediction of the ultimate strength, this value matches with [65] in case of rectangular CFST columns. Values exceeding 40 resulted in a marginal underestimation of the outcomes.

Tao et al. [36] introduced a new model consisting of three-phases to depict the strain hardening/softening behavior of concrete encased in steel tubes as depicted in Figure (°). In the beginning phase (OA), the steel tube and the concrete have minimal interaction, leading to the use of the stress-strain curve for unconfined concrete. Following the initial phase, there's a plateau (from Point A to Point B) that symbolizes the augmented peak strain in concrete due to confinement. In this period, the strength enhancement of the confined concrete is reflected in the simulation due to the interaction between the steel tube and the concrete. After point B, a phase depicting softening and enhanced ductility from confinement is outlined.

2.2.3. Elements, Boundary conditions, and analysis procedures

Four-node shell elements with reduced integration (S4R) and 8-node brick elements with three degrees of freedom of translation at each node (C3D8R) were used to model the steel skin and infill concrete core by Abaqus, respectively.

Two reference points (RP) were modeled by the Abaqus software at the top and the bottom of the column, Figure (6). Each point was connected to all the elements at its column end (steel and

concrete) using the coupling feature in Abaqus. The coupling feature in Abaqus allows connecting two or more elements to a master point so that they move as a single unit. The displacement load was applied to the upper reference point of the column. The two reference points at the top and bottom were identified to be a set for the boundary conditions. This ensured that all parts of any column end will be affected by the displacement load from Abaqus or by the boundary condition together simultaneously. The allowed and restricted degrees of freedom for the column were defined as follows: In the case of buckling model all displacement degrees of freedom were constrained except for the displacement in the loading direction at the upper end of the column. While all rotational degrees are free. In the case axial loading model, all rotational and displacement degrees of freedom were constrained except for the displacement in the loading direction at the upper end of the column.

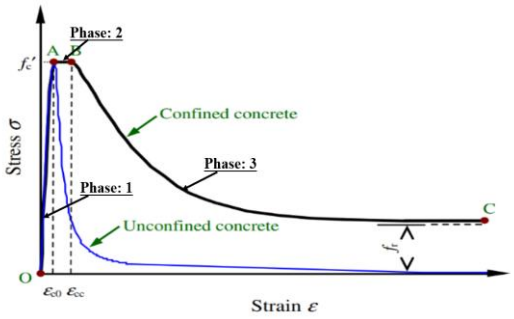

Figure 5- Stress strain curve of confined concrete by Tao et al [36]

CF-BCFSCs are typically tested by applying loads directly using a testing machine. To mitigate the impact of end conditions on the column's behavior, researchers commonly employ rigid end plates and/or stiffeners welded to the ends of the steel skin. However, when tests are conducted without such stiffening tools at the end, as noted in previous study [39], local buckling of the steel tube occurs at the ends, significantly affecting the column's performance. In numerical modeling, the authors simulated the end plates' effect instead of explicitly modeling them. This simulation involves two-steps analysis, as depicted in Figure (6). The first step is the pre-stressing phase, where lateral compressive pressure is applied to the column ends. The second step involves axial displacement loading until failure occurs, determining the ultimate strength. These two steps are considered equivalent to the use of end plates and/or stiffeners at the column ends and loading from the test machine. In both preceding loading steps, the loading was carried out using the static general step available in the Abaqus software, incorporating the activation of geometric nonlinearity.

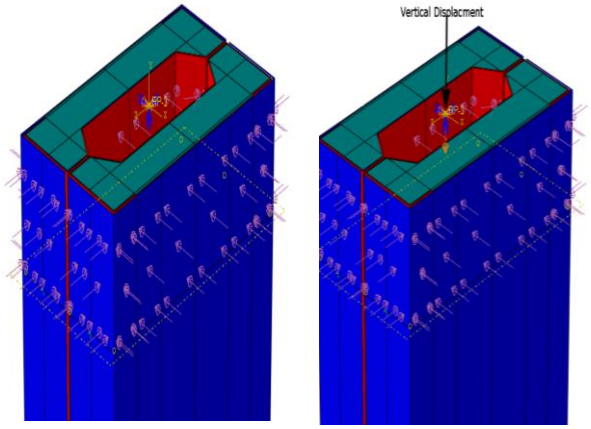

(a) (b)

Figure 6- Step1: Pre-stressing pressure at top and bottom ends, b- Step2: Vertical load through displacement control

2.2.4. Interactions, Meshing, residual stresses, and Initial imperfection

The interaction between steel-to-concrete interfaces and steel components was simulated using a surface-to-surface contact approach in Abaqus [33], Figure (7-b). The contact properties include hard contact allow separation in the normal direction, which means that the surfaces cannot interpenetrate in compression and can separate in tension. In the tangential direction, the Coulomb friction model is used to simulate the contact behavior considered the friction coefficient between the two surfaces. Different values of friction coefficient ranging from 0.25 to 0.6 have been used in previous studies [40, 41]. The authors examined the sensitivity of the friction coefficient of values (0.25, 0.3, 0.4, 0.5, and 0.6) on the axial capacity of composite columns and found that it had a negligible impact. This may be due to less or no slip happening between the steel skin and concrete core because the loading at both parts happens immediately. Based on this finding, the authors of the current study adopted a friction coefficient value of 0.5 for tangential contact because this value produces less convergence

problems and provides a more realistic representation of the actual interaction between steel and concrete in particular, immediately following the initiation of local inflation.

The Abaqus library's ''Beam connector and fastener" technique was used to simulate the fasteners. This method defines the connection between two nodes of different two surfaces using a "beam connector". After that, the real fasteners radius is applied to the beam connector between the two surfaces using 'fastener' tool. The modeling technique for the combined ''beam connector and fastener" is illustrated in Figure (7-a).

To select the optimum mesh size, the authors perform a mesh sensitivity analysis to ensure precise outcomes. The results of various mesh sizes namely 5, 10, 15, and 20 mm revealed negligible differences (≤1%) between 5 mm and 10 mm mesh sizes. A 5% variation was observed between 10 mm and 15 mm mesh sizes. Consequently, a mesh size of 10 mm was selected for both CFS skin profiles and infill concrete core, striking a balance between accuracy and computational efficiency. These results align with the findings reported by Tao et al [35], who indicated that the best element size for the cross-section for these types of columns was B/15 for rectangular columns, where B is the width of the column. The present paper made the elements size in the axial direction equal to the that in the lateral direction (aspect ratio equal 1) to avoid convergence problems according to [35].

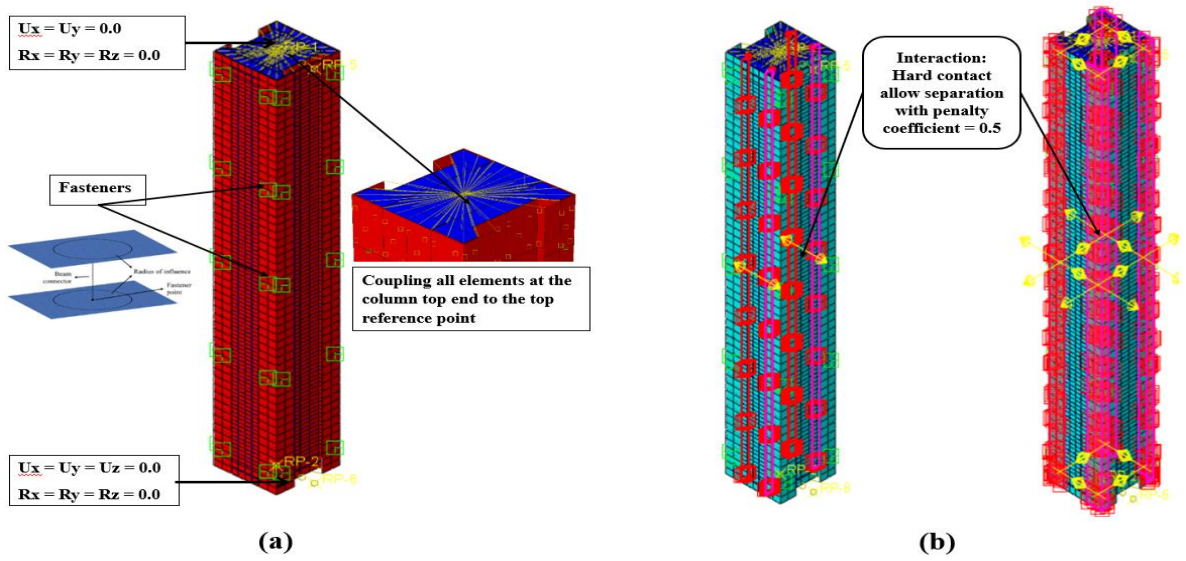

Figure 7- a- Boundary condition, fastener approach and coupling feature, and b- Interaction between steel parts and interaction between steel skin and concrete

Concrete filling is employed to mitigate the impact of residual stresses according to earlier research [25, 35], and as a result, this factor was disregarded in the present finite element simulation. The elastic buckling analysis considered geometric imperfections, with a pinned support as the defined boundary condition depicted in Figure (7-a). Initial imperfections were based on the first buckling mode, and their magnitude was set at 1/300 of the column's length in accordance with EN 1994-1-1 guidelines [4].

3. Results and Discussion

This section includes the results and their discussion, starting with a comparison between the experimental and numerical results to validate the numerical model. This is followed by a comparison of the behavior of different columns in terms of maximum load capacity and ductility, as well as the contribution of both steel and concrete to the load-bearing capacity. Additionally, a cost comparison between them is conducted.

3.1. Verification of the current numerical model

The validation of the numerical model includes three main steps. It begins with a comparison between the experimental and numerical results of the load-displacement curve, followed by a comparison of the maximum load-bearing capacity, and concludes with a comparison of the failure modes.

3.1.1. Load - Displacement curve

The results of the finite element analysis show good agreement with those from experimental tests by Rahnavard et al. [31] and Teoh et al. [31], Figure (8). The same ultimate load is obtained with a difference less than 3 %, and the load-displacement curves are typically the same from the beginning of loading until obtaining the ultimate load. After this, a deviation occurs between the curve resulting from experimental and numerical data. This is manifested by a sudden drop in the curves from the experimental results that do not occur in the numerical curves. This discrepancy can be attributed to the simplification assumed by the authors in modeling the screws using ‘‘Beam connector and fastener” tool in the Abaqus software.

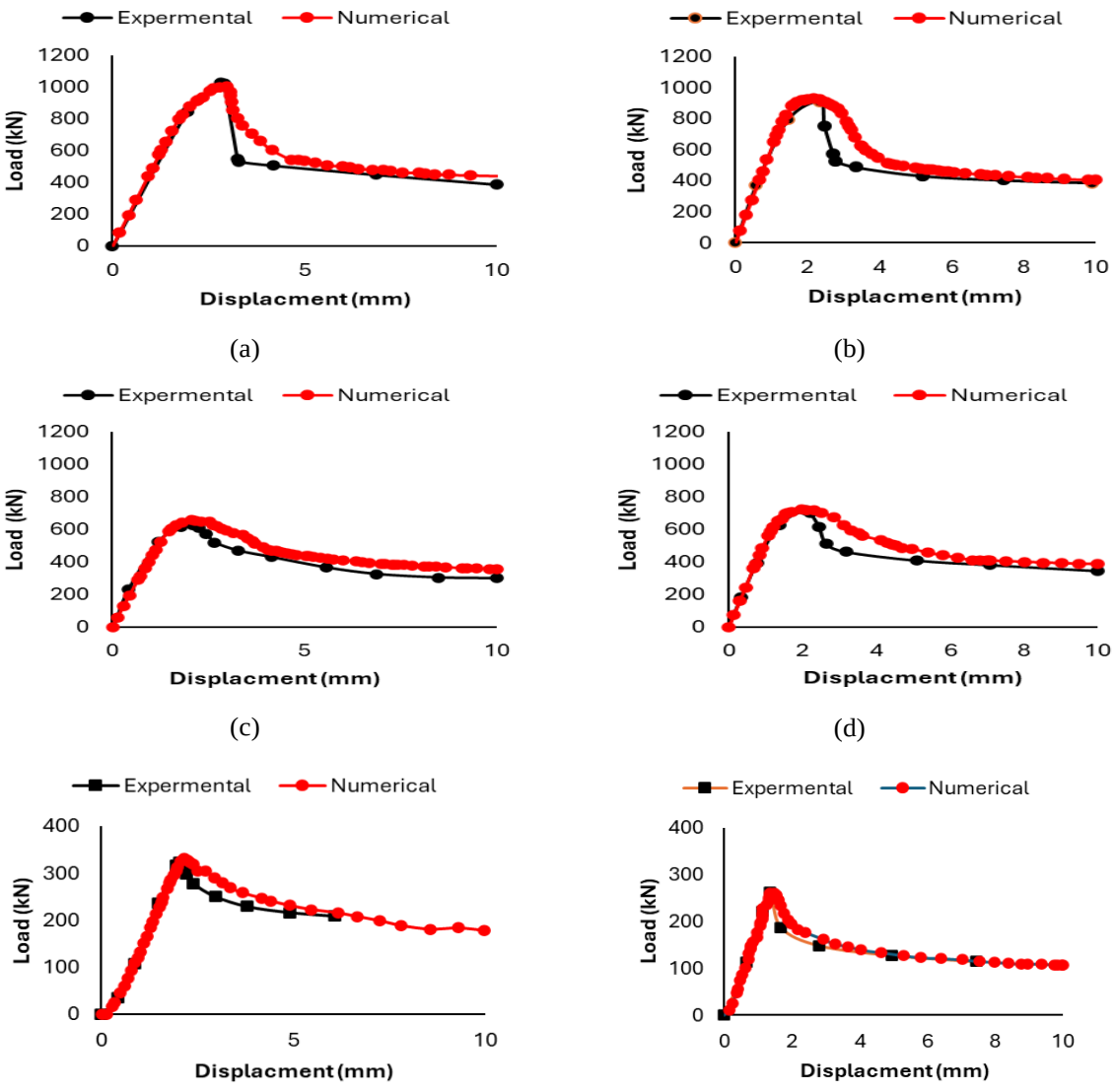

Figure 8- Load-Displacement curves for tested specimens by both of Rahnavard et al [31] and Teoh et al. [34] compared to FE model by the author; (a) S-U+C, (b) S-U+Σ, (c) R-U+Σ, (d) R-U+C and by Teoh et al. [31], (e) 102×51×1-LC20, and (f) 75×40×0.75-LC40

3.1.2. Ultimate load capacity.

Table 2 shows the experimental and numerical results for various columns configurations (S-U+C, S-U+Σ, R-U+Σ, and R-U+C), encompassing ultimate load capacity (Pul), and displacement corresponding to the ultimate load (Δul). The ratio of numerical to experimental ultimate load (PuFE/Puexp) and the displacement ratio (ΔuFE/Δuexp) indicate a generally good agreement, with mean values of 1.011 and 1.002, respectively. The small standard deviations (SD) and coefficients of variance (COV) for both ratios (0.019 and 0.013) affirm the consistency and reliability of the numerical model in capturing the structural response. These findings suggest that the numerical simulation accurately predicts the structural behavior under loading conditions, providing a basis for confidence in the simulation methodology.

Table 2: Comparison between experimental and numerical results

Column	Experimental		Numerical		$\frac{P_{u,FE}}{P_{u,Exp}}$	$\frac{\Delta_{u,FE}}{\Delta_{u,Exp}}$
	P_u kN	Δ_u mm	P_u kN	Δ_u mm		
S-U+C	1021	2.91	1009	2.93	0.988	1.006
S-U+Σ	910	2.33	926	2.29	1.017	0.982
R-U+Σ	625	2.08	647	2.09	1.035	1.004
R-U+C	720	2.05	724	2.08	1.005	1.014
102×51×1-LC20	324	2.04	332	2.16	1.025	1.057
75×40×0.75-LC40	262	1.36	261	1.46	0.996	1.075
Mean	----				1.011	1.002
Standard deviation (SD)	----				0.019	0.013
Coeff of variance (COV)	----				0.019	0.013

3.1.3 Modes of failure

The comparison between experimental and numerical failure modes is illustrated in Figure (9), where the deformed shapes of the tested specimens, as conducted by Rahnavard et al. [31] from (a) to (d) and by Teoh et al. [34] from (e) to (f), are juxtaposed with the finite element (FE) model employed by the authors. Figure 9 shows that visual examination of the deformed shapes allows for a qualitative assessment of the agreement between experimental and numerical results.

This Figure shows that local buckling with distortional buckling is the main mode of failure in all specimen types. Notably, global buckling was not observed at any CF-BCFSCs.

Distortional buckling was observed on the flange of the U-shaped profile in all columns. While local buckling modes were evident in the web of external plain channels (U-shaped profiles) and internal plain channels (C and Σ-shaped profiles). A gap between the internal C profiles in the columns R-U+C emerged as a result of local buckling. Although a gap occurs on the web of the plain channels (U-shaped profiles) between fasteners due to local buckling. This comparative analysis is crucial for validating the accuracy of the finite element model in replicating the observed structural behavior, providing valuable insights into the model's predictive capabilities under various loading conditions. For the tested columns by Teoh et al. [34], the local buckling the major mode of failure in the web and flange, and distortional buckling is obtained at outer flange.

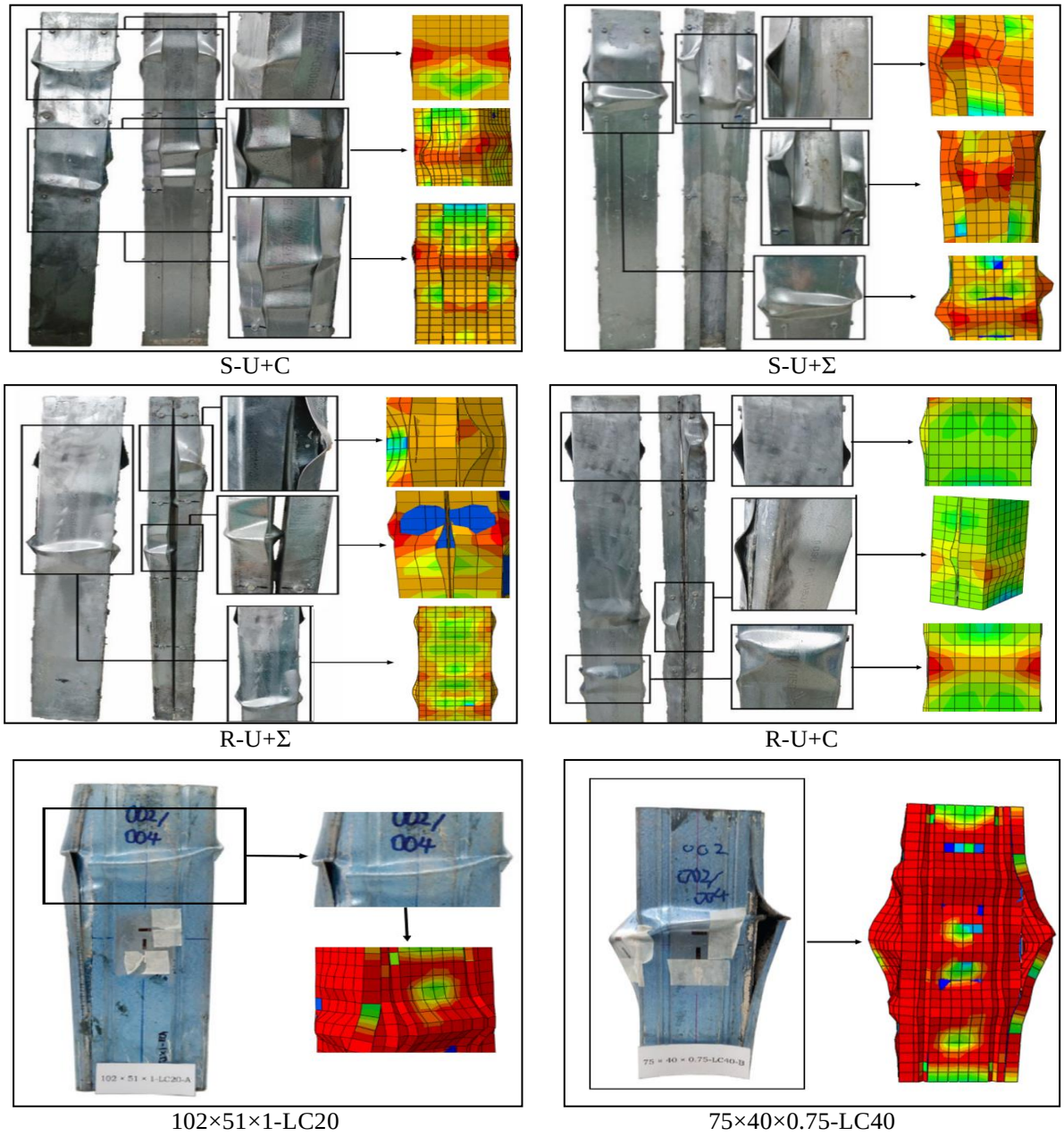

Figure 9- modes of failure for tested column tested by Rahnavard et al [31], and Teoh et al. [34] compared to FE model by the author

3.2 Ultimate Load capacity and Toughness

Figure (10) shows the ultimate load, toughness, and elastic stiffness of the four CF-BCFSCs. It is obvious that the column S-U+C is the strongest of the four columns as it can withstand a maximum load of 1009 kN before it fails. This column surpasses the maximum load it can bear by 9%, 39%, and 56% compared to the other columns, S-U+Σ, R-U+C, and R-U+Σ, respectively. This can be attributed to the larger in the cross-section area of the concrete core in this column by 20%, 79%, and 154 % in comparison to the other columns, in order.

Despite column S-U+C having the highest load bearing capacity, column S-U+Σ exhibits the highest elastic stiffness. This can be attributed to a 5% increase in the steel skin section in this column compared to column S-U+C. Although column S-U+C has a 20% increase in concrete

section area, a comparison of the elastic modulus values for steel and concrete reveals that steel outperforms concrete by 6.5 times in terms of elasticity. Additionally, the higher stiffness of the primary sections comprising the column. Where, the lipped channels with stiffened web (Σ) have a higher stiffness which contribute significantly to increase the column stiffness, and its stiffened web contributes to enhanced resistance to local buckling compared to traditional unstiffened channels. Even though square column S-U+Σshares an identical steel skin area with rectangular column R-U+Σ, it surpasses the latter in elastic stiffness by 30%. This superior performance is linked to a 112% higher concrete section area ratio in column S-U+Σ compared to column R-U+Σ.

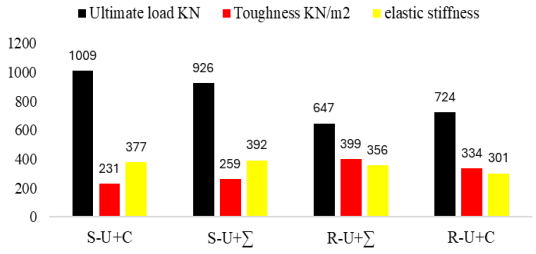

Figure 10- The ultimate load, toughness, and elastic stiffness of four CF-BCFSCs

Figure (10) illustrates the toughness values in kN/m² for the four columns S-U+C, S-U+Σ, R-U+Σ, and R-U+C, corresponding to entries 231, 259, 399, and 334, respectively. It is evident that column R-U+Σ, characterized as the smallest in cross-sectional concrete area, exhibits lower resistance to compressive load. However, it demonstrates the highest toughness. This can be explained by calculating the ratio of the steel section area to the total section area for the four columns, resulting in 6.5%, 8%, 15.5%, and 10.9% in order. It is well-known that an increase in steel content enhances toughness, contrary to the impact of increased concrete, which tends to make the columns more brittle. i.e. Choosing the right column for a specific application depends on the project's requirements. If the designer needs a column that can handle high loads and minimal deflection, S-U+C might be a good choice. However, if impact resistance is a major concern, R-U+Σ might be a better option.

3.2. Comparative Cost-effectiveness

To compare meaningfully between column configuration, the cross-sectional areas of all columns in both steel and concrete must be equal. This is not possible, so the authors used the Egyptian pound (EGP) to ultimate load ratio (EGP/ kN) to compare them as shown in Table-3.

Table3: The ratio of EGP to ultimate load of the columns

Column	P_{uFEM} (kN)	Total cost Egyptian Pound (EGP)	Total cost / Ultimate load (EGP/kN)
R-U+C	1009	1797.47	1.78
S-U+C	926	1830.69	1.98
R-U+Σ	647	1803.48	2.79
S-U+Σ	724	1770.25	2.45

For the R-U+C Configuration, the cost / load ratio is calculated at 1.78, indicating that the column cost is 1.78 times its ultimate load. This ratio is derived from an ultimate bearing load of 1009 kN and a specimen cost 1797.47 EGP. Similarly, the other column configuration. These EGP / kN ratios provide crucial insights into cost-effectiveness and structural efficiency showcasing an efficient utilization of materials of each configuration. The results suggest that the R-U+C Configuration exhibits the lowest EGP-Load ratio, implying superior structural efficiency among the tested Configurations. Further analysis and comparison of these ratios contribute to a deeper understanding of the load-bearing capacity and efficiency of concrete-filled cold-formed steel tube columns.

3.4 Ultimate capacity contribution from steel skin and concrete core

The data in Table 4 is useful for understanding how different materials, Steel skin and concrete core, contribute to the overall capacity (Pu-s and Pu-c) of various scenarios, which could be important in structural analysis contexts.

Table 4: Contribution of the steel skin and concrete core to ultimate Capacity

Column	Concrete area (mm)	Steel Area (mm)	P_{u-FE}	P_{u-c}	P_{u-s}	% contribution of concrete	% contribution of Steel skin
S-U+C	21720	1488	1009	689.7	319.2	68.3	31.6
S-U+Σ	18143	1575.7	926	542.5	383.4	58.5	41.4
R-U+Σ	8543	1575.7	647	261.0	385.9	40.3	59.6
R-U+C	12120	1488	724	369.6	354.3	51.0	48.9

The table allows you to compare the contributions of concrete and steel components in different configurations. For example, in the R-U+Σ configuration, the steel component contributes significantly more (59.66%) compared to the concrete component (40.34%). The percentages provide insights into the relative importance of each material/component in different configurations. The P_{u-c} values range from 261.02kN to 689.77kN, and the P_{u-s} values range from 319.23 kN to 385.98kN. The percentage of concrete contribution values range from 40.34% to 68.36%, while the percentage of steel skin contribution values range from 31.63% to 59.66%. It is interesting to note that the percentage concrete contribution is higher than the steel skin contribution for all cases except for the R-U+Σ where the steel skin contribution is higher than the concrete core It is worth mentioning that this column produced the lowest value for the maximum load, and this is due to a reduction in the concrete cross-sectional area. This explains the higher contribution of the steel skin compared to the concrete core, where the steel area in this column constitutes 15.6% of the total column area. Overall, the data in the table suggests that concrete area is more important in resisting the applied load, and that the S-U+C and S-U+Σ cases are the most effective at resisting the applied load.

4. Conclusions

The current paper discussed numerically the behavior CF-BCFSCs, encompassing four distinct cross-sectional shapes. Additionally, the study determined the influence of individual components, such as steel skin and concrete core, on the ultimate load of the columns, cost comparison between different configuration, and failure modes. The conclusions derived from the research are outlined as follows:

1. The comparison between the proposed numerical model by the authors and the experimental results from Rahnavard et al.'s study [31] reveals a strong and satisfactory correlation where SD and COV equal 0.019 and 0.013 for (P_{uFE}/P_{uExp}) and ($\Delta uFE/\Delta uexp$), respectively. Therefore, this model can be relied upon to simulate columns and predict their behavior in future parametric studies.

2. Local buckling, often accompanied by distortional buckling, is the predominant failure mode in various specimens, while global buckling is not observed in any CF-BCFSCs.

3. Distortional buckling occurs on the flange of outer U-shaped profiles, and local buckling is evident in the web of external plain channels (U-shaped profiles) and internal plain channels (C and Σ-shaped profiles). Local buckling causes gaps between plain channels between fasteners.

4. The Column S-U+C stands out with superior load-bearing capacity, exceeding S-U+Σ, R-U+C, and R-U+Σ by 9%, 39%, and 56%, respectively, attributed to a significantly larger concrete core cross-sectional area by 20%, 79%, and 154%.

5. S-U+Σ, exhibits the highest elastic stiffness due to a 5% increase in the steel skin section, add to this the elastic modulus values underscore steel's superiority over concrete by 6.5.

6. Column R-U+Σ, with the smallest cross-sectional concrete area, demonstrates the highest toughness among the four columns. The steel content in R-U+Σ contributes to its enhanced toughness, emphasizing the importance of choosing the right column based on project requirements, such as load capacity, deflection, and impact resistance.

7. The column S-U+C is the most economic column in producing the least ratio of total cost/ultimate load. This is attributed to the fact that this column has a smaller area of steel and a larger area of concrete. The concrete is significantly more cost-effective than steel, which results in a reduced overall cost for the column.

8. The contribution of concrete core to bearing the ultimate load is significantly greater than the resistance offered by the steel skin. This explains why Column S-U+C has a higher resistance, whereas Column R-U+ Σ has a lower resistance to the ultimate load.

5. References

1. N.E. Shanmugam, and B. Lakshmi, "State of the art report on steel–concrete composite columns", J. of Construction Steel Research, 57(10), 1041–1080, 2001, doi: 10.1016/j.jcsr.2001.03.002.

2. H. Qi, L. Guo, J. Liu, D. Gan, and S. Zhang, "Axial load behavior and strength of tubed steel reinforced-concrete (SRC) stub columns", Thin-Walled Structure, 49(9), 1141–1150, 2011, doi: 10.1016/j.tws.2011.05.013.

3. L.H. Han, W. Bjorhovde, and R. Li, "Developments and advanced applications of concrete-filled steel tubular (CFST) structures: members", J. Construction Steel Research, 100, 211–228, 2014, doi: 10.1016/j.jcsr.2014.07.021.

4. Eurocode 4, Design of Composite Steel and Concrete Structures, Part 1.1: General Rules and Rules for Building, BS EN 1994-1-1: 2004, British Standards Institution, London (UK), 2004.

5. Standards Australia. Bridge design, part 6: steel and composite construction. AS 5100.6-2004. Sydney (Australia), 2004.

6. JGJ 138-2016, Code for Design of Composite Structures, Ministry of Housing and Urban-Rural Development of the People's Republic of China, China, 2016, (in Chinese).

7. ANSI/AISC 360-05, Specification for Structural Steel Buildings, American Institute of Steel Construction, Chicago (IL, USA), 2005.

8. DBJ/T 13-51-2010, Technical Specification for Concrete-Filled Steel Tubular Structures, The Department of Housing and Urban–Rural Development of Fujian Province, Fuzhou (China), 2010, (in Chinese).

9. S. Kazemzadeh Azad, D. Li, and B. Uy, "Axial slenderness limits for austenitic stainless steel-concrete composite columns", J. Construction Steel Research, 166, 105856, 2020, doi: 10.1016/j.jcsr.2020.105856.

10. S. Kazemzadeh Azad, and B. Uy, "Effect of concrete infill on local buckling capacity of circular tubes", J. Construction Steel Research, 165, 105899, 2020, doi: 10.1016/j.jcsr.2019.08.009.

11. S. Kazemzadeh Azad, D. Li, and B. Uy, "Axial slenderness limits for duplex and lean duplex stainless steel-concrete composite columns", J. Construction Steel Research, 172, 106175, 2020, doi: 10.1016/j.jcsr.2020.106175.

12. Ming-Xiang Xiong, Xiong De-Xin, and Richard Liew J.Y., "Axial performance of short concrete filled steel tubes with high- and ultra-high- strength materials", Eng. Struct. 136, 494–510, 2017, doi: 10.1016/j.engstruct.2017.01.037.

13. M.F. Hassanein, Y-B. Shao, M. Elchalakani, and A.M. El Hadidy, "Flexural buckling of circular concrete-filled stainless steel tubular columns", Mar. Struct., 71, 102722, 2020, doi: 10.1016/j.marstruc.2020.102722.

14. M.F. Hassanein, M. Elchalakani, and V.I. Patel, "Overall buckling behaviour of circular concrete-filled dual steel tubular columns with stainless steel external tubes", Thin-Walled Struct., 115, 336–348, 2017, doi: 10.1016/j.tws.2017.03.029.

15. M.A. Dabaon, M.H. El-Boghdadi, and M.F. Hassanein, "Experimental investigation on concrete-filled stainless steel stiffened tubular stub columns", Eng. Struct., 31(2), 300–307, 2009, doi: 10.1016/j.engstruct.2008.09.017.

16. M.A. Dabaon, S. El-Khoriby, M. El-Boghdadi, and M.F. Hassanein, "Confinement effect of stiffened and unstiffened concrete-filled

stainless steel tubular stub columns", J. Construction Steel Research, 65(8-9), 1846–1854, 2009, doi: 10.1016/j.jcsr.2009.05.012.

17. L.-H. Han, Z. Tao, H. Huang, and X.-L. Zhao, "Concrete-filled double skin (SHS outer and CHS inner) steel tubular beam–columns", Thin-Walled Structures, 42(9), 1329–1355, 2004, doi: 10.1016/j.tws.2004.01.008.

18. L.-H. Han, Q.-X. Ren, and W. Li, "Tests on stub stainless steel–concrete–carbon steel double-skin tubular (DST) columns", Journal of Constructional Steel Research, 67(3), 437–452, 2011, doi: 10.1016/j.jcsr.2010.10.008.

19. B. Uy, Z. Tao, and L.-H. Han, "Behaviour of short and slender concrete-filled stainless steel tubular columns", Journal of Constructional Steel Research, 67(3), 360–378, 2011, doi: 10.1016/j.jcsr.2010.09.004.

20. W. Li, Q.-X. Ren, L.-H. Han, and X.-L. Zhao, "Behaviour of tapered concrete-filled double skin steel tubular (CFDST) stub columns", Thin-Walled Structures, 57, 37–48, 2012, doi: 10.1016/j.tws.2012.03.017.

21. F.-C. Wang, L.-H. Han, and W. Li, "Analytical behavior of CFDST stub columns with external stainless-steel tubes under axial compression", Thin-Walled Structures, 127, 756–768, 2018, doi: 10.1016/j.tws.2017.11.034.

22. I. Nishiyama, S. Morino, K. Sakino, et al., "Summary of Research on Concrete-Filled Structural Steel Tube Column System Carried Out under the US-Japan Cooperative Research on Composite and Hybrid Structures", Building Research Institute, Ibaraki Prefecture, Japan.

23. M. H. Lai, and J. C. M. Ho, "A theoretical axial stress-strain model for circular concrete-filled steel-tube columns", Engineering Structures, 125, 124–143, 2016, doi: 10.1016/j.engstruct.2016.06.019.

24. J.-Y. Zhu, and T.-M. Chan, "Behaviour of polygonal-shaped steel-tube columns filled with high-strength concrete", Proceedings of the Institution of Civil Engineers - Structures and Buildings, 171(2), 96–112, 2017, doi: 10.1680/jstbu.15.00106.

25. F. Aslani, B. Uy, Z. Wang, and V. Patel, "Confinement models for high strength short square and rectangular concrete-filled steel tubular columns", Steel and Composite Structures, 22(5), 937–974, 2016, doi: 10.12989/scs.2016.22.5.937.

26. F. X. Ding, Z. Li, S. Cheng, and Z. W. Yu, "Composite action of hexagonal concrete-filled steel tubular stub columns under axial loading", Thin-Walled Structures, 107, 502–513, 2016, doi: 10.1016/j.tws.2016.06.003.

27. F. X. Ding, Z. Li, S. Cheng, and Z. W. Yu, "Composite action of octagonal concrete-filled steel tubular stub columns under axial loading", Thin-Walled Structures, 107, 453–461, 2016, doi: 10.1016/j.tws.2016.06.005.

28. E. Ellobody, Ben Young, and Dennis Lam, "Behaviour of normal and high strength concrete-filled compact steel tube circular stub columns", J. Construction Steel Research, 62(7), 706–715, 2006, doi: 10.1016/j.jcsr.2005.09.006.

29. E. Ellobody, Ben Young, "Numerical simulation of concrete encased steel composite columns", J. Construction Steel Research, 67(2), 211–222, 2011, doi: 10.1016/j.jcsr.2010.09.013.

30. E. Ellobody, Ben Young, and Dennis Lam, "Eccentrically loaded concrete encased steel composite columns", Thin Walled Struct., 49(1), 53–65, 2011, doi: 10.1016/j.tws.2010.08.013.

31. R. Rahnavard, H. D. Craveiro, R. A. Simões, L. Laím, and A. Santiago, "Buckling resistance of concrete-filled cold-formed steel (CF-CFS) built-up short columns under compression", Thin-Walled Structures, doi: 10.1016/j.tws.2022.107973.

32. R. Rahnavard, H. D. Craveiro, R. A. Simões, L. Laím, and A. Santiago, "Concrete-filled cold-formed steel (CF-CFS) built-up columns under compression: Test and design", Thin-Walled Structures, doi: 10.1016/j.tws.2022.107997.

33. Abaqus Analysis User's Guide, Version 6.17, Dassault Systèmes Simulia, USA, 2017.

34. Teoh Keat, Chua Yie, Pang Sze, and Kong Sih, "Experimental investigation of

lightweight ggregate concrete-filled cold-formed built-up box section (CFBBS) stub columns under axial compression", Engineering Structures 279 (2023) 115630.

35. D. Chen, H. Wu, J. S Wei, S. L Xu, and Q Fang, "Nonlinear visco-hyperelastic tensile constitutive model of spray polyurea within wide strain-rate range", International Journal of Impact Engineering, doi: 10.1016/j.ijimpeng.2021.103210.

36. Zhong Tao, Zhi-Bin Wang, and Qing Yu, "Finite element modelling of concrete-filled steel stub columns under axial compression", Journal of Constructional Steel Research, doi: 10.1016/j.jcsr.2013.03.001.

37. V.K. Papanikolaou, A.J. Kappos, "Confinement-sensitive plasticity constitutive model for concrete in triaxial compression", Int J Solids Struct 2007;44(21):7021–48, doi: 10.1016/j.ijsolstr.2007.02.015

38. T. Yu, J.G. Teng, Y.L. Wong, S.L. Dong, "Finite element modeling of confined concrete-I: Drucker–Prager type plasticity model", Eng Struct 2010;32(3):665–79, doi: 10.1016/j.engstruct.2009.11.003.

39. T. Yamamoto, J. Kawaguchi, S. Morino, "Experimental study of scale effects on the compressive behavior of short concrete-filled steel tube columns", Proceedings of the Fourth International Conference on Composite Construction in Steel and Concrete, Banff, Alberta, Canada; 2000. p. 879–90.

40. S.P. Schneider, "Axially loaded concrete-filled steel tubes", J Struct Eng, ASCE 1998;124(10):1125,doi:0.1061/(ASCE)0733-9445(1998)124:10(1125).

41. L.H. Han, G.H. Yao, Z. Tao, "Performance of concrete-filld thin-walled steel tubes under pure torsion", Thin-Walled Struct. 2007; 45(1):24–36,doi:1016/j.tws.2006.03.003.